General Disclaimer

One or more of the Following Statements may affect this Document

- This document has been reproduced from the best copy furnished by the organizational source. It is being released in the interest of making available as much information as possible.

- This document may contain data, which exceeds the sheet parameters. It was furnished in this condition by the organizational source and is the best copy available.

- This document may contain tone-on-tone or color graphs, charts and/or pictures, which have been reproduced in black and white.

- This document is paginated as submitted by the original source.

- Portions of this document are not fully legible due to the historical nature of some of the material. However, it is the best reproduction available from the original submission.

70-00877

Department of AERONAUTICS and ASTRONAUTICS
STANFORD UNIVERSITY

Theoretical Considerations of Some Nonlinear Aspects of Hypersonic Panel Flutter

by

S. C. McIntosh
and
J. I. Lerner

Third Annual Report

NASA Grant NGR 05-020-102

1 September 1967 to 31 August 1968

32

Theoretical Considerations of Some Nonlinear Aspects of Hypersonic Panel Flutter

by

S. C. McIntosh

and

J. I. Lerner

Third Annual Report

NASA Grant NGR 05-020-102

1 September 1967 to 31 August 1968

TABLE OF CONTENTS

		Page
I.	INTRODUCTION	1
II.	EFFECTS OF AERODYNAMIC NONLINEARITIES ON POSTCRITICAL RESPONSE.	2
III.	EFFECT OF AERODYNAMIC NONLINEARITIES ON STABILITY.	9
IV.	EFFECT OF AN UNSTEADY BOUNDARY LAYER ON PANEL FLUTTER.	11
V.	CONCLUDING REMARKS	19
	REFERENCES	20
	FIGURES.	21

NOMENCLATURE

a	Panel chord
$\bar{a}_k$	Modal amplitude for transverse displacement
a_k	Dimensionless modal amplitude, $\bar{a}_k/h$
$\bar{b}_0, \bar{b}_R$	Modal amplitudes for in-plane displacement
D	Plate modulus, $Eh^3/12(1-\nu^2)$
E	Modulus of elasticity
$(F_z)_k$	Generalized force associated with k^{th} transverse mode
h	Panel thickness
h_0	Local total enthalpy, local enthalpy + $(u^2+v^2)/2$
k	Wave number, $2\pi/a$
K	Running spring constant, panel in-plane restraint spring
M	Free-stream Mach number
N	Number of assumed modes for transverse displacement
p	Pressure
p_∞	Free-stream static pressure
$\overline{\Delta p}$	Static pressure difference across panel; positive if cavity pressure exceeds free-stream static pressure
Δp	Dimensionless static pressure difference, $\overline{\Delta p}\ a^4/Dh$
q	Free-stream dynamic pressure, $\rho U^2/2$
$\bar{q}$	Heat-transfer rate
$\bar{R}_x$	Applied in-plane load
$\bar{R}_{xu}$	Applied in-plane load varying with time
R_x, R_{xu}	Dimensionless in-plane loads - dimensional loads referred to D/a^2
t	Time

u	Local velocity component in x direction
U	Free-stream speed
v	Local velocity component in y direction
$\bar{w}$	Transverse displacement
$\tilde{w}$	Amplitude of transverse displacement: $\bar{w}(x,t) = \tilde{w}(x)e^{i\omega t}$
x	In-plane (axial) coordinate
y	Transverse coordinate, Sec. IV
z	Transverse coordinate
α'	In-plane restraint parameter, $K/[K+Eh/a(1-\nu^2)]$
γ	Gas constant for free-stream ($\gamma = 1.4$)
δ	Viscous thermal-layer thickness measured from x axis
δ^*	Mass displacement thickness defined by Eq. (4.10)
δ_1	Density defect thickness defined by Eq. (4.13)
δ_h^*	Enthalpy displacement thickness defined by Eq. (4.14)
θ	Momentum defect thickness defined by Eq. (4.11)
θ_h	Enthalpy defect thickness defined by Eq. (4.12)
λ	Dimensionless dynamic-pressure parameter, $2qa^3/MD$
μ	Dimensionless mass ratio, $\rho a/\rho_m h$
ν	Poisson's ratio
ρ	Free-stream mass density
ρ_m	Panel mass density
σ_x	Panel axial stress - see Eq. (2.5)
τ	Dimensionless time, $t(D/\rho_m h a^4)^{1/2}$
$\bar{\tau}$	Fluid shear stress
ω	Frequency
$(\dot{})$	Derivative of dimensionless quantity with respect to τ

I. INTRODUCTION

This report presents a summary of the third year's research activity under NASA Grant NGR 05-020-102, monitored technically by the Nonsteady Phenomena Branch of Ames Research Center. The goals of this research program are twofold:

(1) to study in a systematic manner the effects on panel response and stability of nonlinear, nonviscous aerodynamic loading at hypersonic Mach numbers, and

(2) to determine theoretically the effects of a turbulent boundary layer on the aerodynamic loading of an oscillating panel.

The following sections present results from a study of stability and and postcritical response of a panel of infinite width on hinged supports, including a critical evaluation of the important nonlinear aerodynamic terms, and the initial results from the study of the effects of a turbulent boundary layer on the aerodynamic loading of an oscillating panel of infinite width. A concluding section discusses plans for the next year.

II. EFFECTS OF AERODYNAMIC NONLINEARITIES ON POSTCRITICAL RESPONSE

In Ref. 1 are presented the equations of motion for a panel of infinite width (a plate-column) on hinged supports with both geometric and aerodynamic nonlinear terms (see Fig. 1). The panel middle-surface displacement $\bar{w}(x,t)$ is approximated in space by a series of assumed modes with time-dependent modal amplitudes, and a set of second-order quasi-linear ordinary differential equations in time is derived for these modal amplitudes (cf. Eqs. (2.14) of Ref. 1). These equations are then integrated from given initial conditions to produce a time history of the panel displacement. For values of λ greater than the critical value, there is in general an initial transient, followed by a limit-cycle oscillation of constant amplitude and frequency. (For certain compressive values of R_x this picture is altered somewhat - see Ref. 2.) The effects of nonlinear aerodynamic loading were evaluated by comparing this limit-cycle frequency and amplitude to those obtained from a similar integration with linear aerodynamic loading. It was soon found that only certain of the aerodynamic nonlinear terms would possibly be significant for parameter ranges anywhere near those found in practice. On the other hand, the term deemed likely to be most significant of all the nonlinear ones - that proportional to $(\partial\bar{w}/\partial x)^2$ - does no net work over a cycle if at every point on the panel the displacement into the flow (+w) is a mirror image of the displacement into the cavity (-w). It was therefore decided to include in the analysis the piston-theory aerodynamic term proportional to $(\partial\bar{w}/\partial x)^3$, which does work over such a cycle, to be certain that significant effects would not be left out. The contribution of this term to the pressure difference

on the panel is

$$(p-p_\infty)_{cubic} = \frac{(\gamma+1)qM}{6}\left(\frac{\partial \bar{w}}{\partial x}\right)^3 \tag{2.1}$$

with the contribution to the generalized aerodynamic forces

$$(F_z)_{k,cubic} = -\frac{(\gamma+1)qM}{6}\int_0^a \left(\frac{\partial \bar{w}}{\partial x}\right)^3 \sin\frac{k\pi x}{a}\,dx \tag{2.2}$$

This expression is readily integrated, with $(\partial\bar{w}/\partial x)^3$ written in terms of the assumed modes, to provide the additional terms in the equations for the modal amplitudes. With only the terms studied subsequently, these equations are

(continued next page)

$$\frac{1}{2}\ddot{a}_k+\frac{1}{2}\pi^2k^2(R_x+\pi^2k^2)a_k+\frac{3}{2}\pi^4k^2\alpha' a_k\sum_{n=1}^{N}n^2a_n^2+\lambda\sum_{n=1}^{N}\frac{kn[1-(-1)^{k+n}]}{k^2-n^2}a_n+\frac{1}{2}(\lambda\frac{\mu}{M})^{\frac{1}{2}}\dot{a}_k-\frac{[1-(-1)^k]}{k\pi}\Delta p$$

$$+\frac{(\gamma+1)\pi k}{4}\lambda M\frac{h}{a}\sum_{m,n=1}^{N}\frac{mn(k^2-m^2-n^2)[1-(-1)^{k+m+n}]}{[k^2-(m-n)^2][k^2-(m+n)^2]}a_m a_n+\frac{(\gamma+1)\pi}{8}M\frac{\dot{h}}{a}(\lambda\frac{\mu}{M})^{\frac{1}{2}}\left[\sum_{\substack{m,n=1\\m+n=k}}^{N}ma_m\dot{a}_n+\sum_{\substack{m,n=1\\m-n=k}}^{N}(na_n\dot{a}_m-ma_m\dot{a}_n)\right]$$

$$-\frac{(\gamma+1)k}{2\pi}\frac{\mu}{M}M\frac{h}{a}\sum_{m,n=1}^{N}\frac{mn[1-(-1)^{k+m+n}]}{[k^2-(m-n)^2][k^2-(m+n)^2]}\dot{a}_m\dot{a}_n+\frac{\pi^2(\gamma+1)k}{48}\lambda(M\frac{h}{a})^2\sum_{\ell,m,n=1}^{N}[1-(-1)^{k+\ell+m+n}]\Big\{[k^2-(\ell-m-n)^2]^{-1}$$

$$+2[k^2-(\ell-m+n)^2]^{-1}+[k^2-(\ell+m+n)^2]^{-1}\Big\}a_\ell a_m a_n=0\ ,$$

$$k=1,2,\ldots,N \qquad (2.3)$$

The third summation term above, which is quadratic in the modal amplitudes, is the generalized force associated with the aerodynamic loading proportional to $(\partial\bar{w}/\partial x)^2$. There follow, in order, generalized forces resulting from the aerodynamic loading proportional to $(\partial\bar{w}/\partial x)(\partial\bar{w}/\partial t)$, to $(\partial\bar{w}/\partial t)^2$, and finally to $(\partial\bar{w}/\partial x)^3$. The parameters are arranged so as to illustrate that one new parameter appears with the introduction of these nonlinear aerodynamic loadings - Mh/a.

The in-plane restraint parameter α' can be written as follows:

$$\alpha' = \frac{K}{K + \dfrac{Eh}{a(1-\nu^2)}} \tag{2.4}$$

This form is used simply to show that α' is made up of contributions from two "springs" - one representing the degree of in-plane restraint, the other representing the panel's own resistance to tension or compression (without buckling). (See Eq. (2.9) of Ref. 1.) The variation of α' with K is plotted in Fig. 2 for representative values of E, ν, and h/a.

The postcritical panel response with linear aerodynamic loading was compared to that with nonlinear aerodynamic loading for various combinations of the nonlinear aerodynamic terms. The parameter Mh/a was for the most part fixed at 0.05 (say, $h/a = 0.005$ and $M = 10.0$).

A typical comparison is illustrated in Figs. 3 and 4, for $\lambda = 550$, $R_x = 0$, $\alpha' = 1.0$, and other system parameters given in the captions. The nonlinear aerodynamic terms used in obtaining Fig. 4 were those proportional to $(\partial\bar{w}/\partial x)^2$ and $(\partial\bar{w}/\partial x)(\partial\bar{w}/\partial t)$. These two terms were found to be the only ones affecting significantly the limit-cycle amplitude and frequency, at least for realistic values of the system parameters. The

term proportional to $(\partial\bar{w}/\partial t)^2$ would undoubtedly have an effect if μ were large, as would the term proportional to $(\partial\bar{w}/\partial x)^3$ if Mh/a were large (say, 1.0 or greater). As can be verified from the figures, the primary effect of the nonlinear terms is to cause a mean displacement of the panel into the cavity. This is explained by the action of the aerodynamic term proportional to $(\partial\bar{w}/\partial x)^2$, which provides an overpressure, tending to push the panel into the cavity, as a result of any deviation of the panel from its flat initial position. This effect is further illustrated in Fig. 5, which compares the growth in peak limit-cycle amplitudes at $x/a = 0.75$ as a function of λ for linear and nonlinear aerodynamic loading. For the linear case, of course, the panel oscillates as far out into the flow as it does into the cavity; with nonlinear aerodynamic loading, the peaks into the cavity (negative w) are greater, and those into the flow (positive w) are less. However, the changes are quite small, even well into the supercritical regime, and the frequency of the oscillation is virtually unchanged by the nonlinear aerodynamic loading.

The in-plane restraint parameter α' is the key parameter governing the stabilizing influence of the panel geometric nonlinearity. For values of this parameter less than unity, one might expect the nonlinear aerodynamic terms to have a greater effect. A linear-nonlinear aerodynamic comparison is shown in Fig. 6 for $\lambda = 550$ and varying α'. It can readily be observed that the nonlinear aerodynamic terms do have a relatively greater effect, to the extent that the peak displacement into the external flow at $x/a = 0.75$ is reduced some 23% for $\alpha' = 0.1$. On the other hand, corresponding peak displacement into the cavity is increased by very little. In sum, the increase of the peak displacement with linear

aerodynamic loading as α' is reduced keeps pace with the increased effect of nonlinear aerodynamic loading. The frequency is unchanged as well.

Another important consideration is the changes in stress caused by nonlinear aerodynamic loading. The stress in the panel can be written in terms of modal amplitudes and other system parameters as (Ref. 2)

$$\sigma_x = \frac{1-\nu^2}{E(h/a)^2}\bar{\sigma}_x = \frac{z}{h}\sum_{k=1}^{N}(k\pi)^2 a_k \sin\frac{k\pi x}{a} + \frac{R_x}{12} + \frac{\alpha'}{4}\sum_{k=1}^{N}(k\pi a_k)^2 \tag{2.5}$$

The maximum or minimum of σ_x at any instant of time occurs for $z=\pm h/2$, so it is seen that the stress distributions for maximum and minimum stress will plot as curves symmetric about a mean, the stress due to stretching, given by the constant terms in Eq. (2.5). Fig. 7 compares these stress distributions in the panel, at the instant the displacement at $x/a=0.75$ reaches a peak, for $\alpha' = 0.1$ and $\lambda = 550$. The maximum tensile and compressive stresses occur at $x/a \simeq 0.85$, and the nonlinear aerodynamic loading increases these stresses by at most 5%. For aluminum, $E \simeq 10^7$ and $\nu = 1/3$; with $h/a = 0.005$, a stress σ_x of 60 corresponds to a dimensional stress $\bar{\sigma}_x$ of 16,900 psi, which is well below the yield stresses of approximately 60,000 psi in tension and 40,000 psi in compression.

To test the accuracy of the numerical integration, the equations of motion were integrated backward in time with initial conditions given by the state of the panel at some instant during a previous calculation.

The panel motions with time could then be compared. The parameter in the numerical-integration subroutine that governs the acceptable relative error between integration steps was kept small enough so that no significant differences arose between integrating forward and backward in time.

A key assumption in the derivation of the panel equations of motion is that $(\partial\bar{w}/\partial x)^2$ is much less than unity. In terms of modal amplitudes, this is

$$\left(\frac{\partial\bar{w}}{\partial x}\right)^2 = \left(\frac{h}{a}\right)^2\left(\sum_{k=1}^{N} k\pi a_k \cos\frac{k\pi x}{a}\right)^2 \qquad (2.6)$$

This distribution was calculated for various large-amplitude panel states. Generally, the largest values are at $x=a$; the largest of these calculated is approximately 0.01, which was calculated from the mode shape corresponding to the nonlinear-aerodynamic stress distribution of Fig. 7. Values for other cases and over other portions of the panel are much smaller, so it is clear that the computed results do not violate this "moderate-rotation" assumption.

It appears therefore that the influence on postcritical response of nonlinear aerodynamic loading of the type considered here is minor. The postcritical panel motion is such that terms quadratic in $\partial\bar{w}/\partial x$ do virtually no net work over a cycle; the cubic terms, which would do work over a cycle, are not important unless the parameter Mh/a is unrealistically large. It was observed, however, that transient motions - such as those that occur postcritically before the steady-state amplitude and frequency are attained - were affected markedly by the nonlinear aerodynamic terms.

III. EFFECT OF AERODYNAMIC NONLINEARITIES ON STABILITY

As a result of the observations of Sec. II, it was decided to shift emphasis to a study of the panel response when the applied in-plane load is varied across a linear stability boundary, as was done to induce flutter experimentally (Ref. 3). Incorporating a time-varying in-plane load in the panel equations of Sec. II is straightforward. The constant in-plane applied load $\bar{R}_x$ is replaced by a constant load plus a time-varying load $\bar{R}_{xu}(t)$, and the potential of the conservative external loads on the panel becomes (see Eq. (2.4) of Ref. 1)

$$\Phi_e = \bar{R}_x \bar{b}_R + (\bar{R}_x + \bar{R}_{xu})\bar{b}_0 - \frac{1}{2} K \bar{b}_0^2 \tag{3.1}$$

Subsequent steps follow exactly those described in Sec. II of Ref. 1, with the final result that the term involving R_x in Eq. (2.3) of this report becomes

$$\frac{1}{2}\pi^2 k^2 [R_x + (1-\alpha')R_{xu} + \pi^2 k^2] a_k \tag{3.2}$$

A typical variation of the in-plane applied load is illustrated in Fig. 8. The panel is initially set in motion at point A, on the stable side of the linear stability boundary. Then the in-plane load is decreased to point B, on the unstable side of the boundary, and held there until the motion of the panel is established. Finally, the load is increased again to point A, where the motion of the panel either dies out or reaches a limit cycle, depending on the influence of the nonlinear aerodynamic terms.

The number of significant nonlinear aerodynamic terms was reduced to the same two that were described in Sec. II. Fig. 9 presents a time

history of the displacement at $x/a = 0.75$ for values of λ and in-plane load corresponding to point A in Fig. 8. In this case the motion is that which results after the in-plane load has been increased from the value corresponding to point B in Fig. 8. Thus the energy imparted to the panel while at point B is sufficient to produce an instability at point A, where the panel would be stable in the absence of nonlinear aerodynamic loading. Figures 10-17 illustrate the panel mode shapes at various moments during the time history of Fig. 9. Note that as the panel displacement becomes predominantly negative the mode shape undergoes a transition from that shape usually associated with panel flutter to a shape similar to the fundamental buckling mode. This is the same behavior noted in Ref. 2 for panel motions with linear aerodynamic loading in the region around point C in Fig. 8.

Stress distributions and $(\partial\bar{w}/\partial x)^2$ distributions were calculated for points corresponding to the peak negative and peak positive displacements in Fig. 9. In neither of these cases did the maximum absolute value of the stress or the maximum value of $(\partial\bar{w}/\partial x)^2$ exceed the respective maxima discussed in Sec. II.

IV. EFFECT OF AN UNSTEADY BOUNDARY LAYER ON PANEL FLUTTER

Prior to beginning a theoretical investigation of the effects of an unsteady boundary layer on panel flutter a study was conducted of some of the recent publications dealing with viscous effects over fluctuating surfaces. These works cover the period of the past ten years when most of the definitive efforts to include viscous effects in unsteady aerodynamics took place.

The theoretical work of Benjamin (Ref. 4) is worth noting as it represents what appears to be the first effort to include the effects of an actual boundary-layer profile of velocity in attempting to predict the pressure and shear stress on an infinite wall with small-amplitude sinusoidal travelling waves. In considering a two-dimensional incompressible flow using the analytical tools of hydrodynamic stability theory, he was able to show that previous idealized models of the boundary layer which treat the viscous region as an inviscid shear layer are inadequate near the surface where the no-slip condition must be satisfied and at the "critical layer" where fluid particle speed is equal to the wave speed.

Recent papers by Rattayya and Volk (Ref. 5) and Zeydel (Ref. 6) attempted to improve upon the earlier shear-flow models of the boundary layer, where the velocity profile is constant and the pressure is determined from linearized potential-flow theory. In both of these papers the authors divided the boundary layer into N thin sublayers where the velocity and density are assumed constant so that the flow is irrotational in each layer. Zeydel applied this technique to a finite-chord panel by use of the Fourier integral and showed how the Ritz-Galerkin technique

could be used to obtain the generalized aerodynamic force acting on the panel.

Perhaps the most ambitious study to date is the work of McClure (Ref. 7) who attempted to consider the general problem involving viscosity, compressibility, and turbulence in a sophisticated analysis that raised more questions than it answered. In an approximate analysis of the flutter of a finite panel he used formulas for the pressure due to a travelling wave. With a two-mode Galerkin analysis he was able to obtain much better agreement for the flutter boundary with experiments than when using potential-flow theory.

The current level of physical understanding of the influence of the boundary layer in aeroelastic calculations is explained by Ashley and Landahl (Ref. 8). In a discussion devoted to qualitative estimates of the effect of an attached boundary layer on an unsteady flow, they identify a quasi-steady increase of body thickness due to the boundary-layer displacement thickness, a dynamic effect due to rate of change of displacement thickness, and boundary-layer "compliance" effects, which are significant in the case of panel flutter, where the outer edge of the boundary layer does not follow the surface deformations exactly, and where the boundary layer does not act like a more-or-less rigid extension of the panel.

After gaining some appreciation for the problems associated with an analytical investigation of an unsteady boundary layer through familiarization with the pertinent literature, it was decided to attempt a completely novel approach in order to determine the viscous effects on panel flutter. The previous efforts in this area are unsatisfactory because the boundary

layer is oversimplified or because the analysis is too complicated to apply in a practical situation. The idealized models used in the study of Rattayya and Volk and the report by Zeydel do not reasonably depict the viscous shear mechanisms and boundary conditions appropriate to viscous flow, while the asymptotic analysis of McClure is rather difficult to apply. These shortcomings might best be overcome by using the integral approach to handle the unsteady turbulent boundary-layer equations in a manner analogous to the method that has had some degree of success in predicting viscous effects in steady flow. The work of Rasmussen and Karamcheti (Ref. 9) in predicting viscous effects in the hypersonic flow through a nozzle is an example of this method used in steady flow.

The following problem will be studied: The surface pressure distribution over an oscillating panel of finite chord a and infinite span is to be determined by simultaneously solving for the turbulent boundary layer adjacent to the panel and the inviscid flow in the remainder of the fluid region. We assume that the panel transverse displacement $\bar{w}(x,t)$ is a known function of axial position, x, and time, t, and we would like to predict the resulting pressure distribution in the presence of an unsteady boundary layer of thickness $\delta(x,t)$ to be determined in the course of the analysis. The pressure distribution thus found is to be compared to what would be predicted by unsteady potential-flow theory. The flow geometry and Cartesian coordinate system are shown in Fig. 18. A set of integral conservation equations that applies to the region of the turbulent boundary layer $y \leq \delta(x,t)$ can be obtained from the differential form of the boundary-layer equations written for laminar flow. Since the velocity and enthalpy profiles do not explicitly appear in the

integral equations, these integral forms of the equations apply to laminar and turbulent boundary layers alike provided no statement is made about the stress at the panel surface, $\bar{\tau}_s$, or the heat flux at the surface, $\bar{q}_s$.

The differential form of the boundary-layer equations used as the starting point for the analysis is written below:

$$\frac{\partial \rho}{\partial t} + \frac{\partial}{\partial x}(\rho u) + \frac{\partial}{\partial y}(\rho v) = 0 \tag{4.1}$$

$$\frac{\partial}{\partial t}(\rho u) + \frac{\partial}{\partial x}(\rho u^2) + \frac{\partial}{\partial y}(\rho uv) = -\frac{\partial p}{\partial x} + \frac{\partial \bar{\tau}}{\partial y} \tag{4.2}$$

$$\frac{\partial p}{\partial y} = 0 \qquad \text{(leading to } p = p(x,t)) \tag{4.3}$$

Energy:

$$\frac{\partial}{\partial t}(\rho h_0) + \frac{\partial}{\partial x}(\rho u h_0) + \frac{\partial}{\partial y}(\rho v h_0) = \frac{\partial p}{\partial t} + \frac{\partial}{\partial y}(\bar{\tau}u - \bar{q}) \tag{4.4}$$

where the variables are defined in the Nomenclature.

The integral form of the boundary-layer equations can be found by integrating the differential equations with respect to y from the panel surface $\bar{w}$ to the edge of the thickest viscous layer adjacent to the panel surface. In actuality there are two layer thicknesses to consider; the velocity thickness Δ_v , which relates to the frictional effects, and the thermal thickness Δ , which relates to heat-transfer effects. For the moment let us assume that Δ is the larger of the two and use $y = \delta = \bar{w} + \Delta$ as the upper limit of integration. The boundary conditions for the integration are

$$u(x,\bar{w},t) = 0 \qquad u(x,\delta,t) = u_e(x,t)$$

$$v(x,\bar{w},t) = v_s(x,t) = \frac{\partial \bar{w}}{\partial t} \text{ (known)} \qquad v(x,\delta,t) = v_e(x,t)$$

$$\bar{\tau}(x,\bar{w},t) = \bar{\tau}_s \qquad \rho(x,\delta,t) = \rho_e(x,t)$$

$$\bar{q}(x,\bar{w},t) = \bar{q}_s \qquad h_0(x,\delta,t) = h_{0_e}(x,t)$$

$$\rho(x,\bar{w},t) = \rho_s(x,t) \qquad \bar{\tau}(x,\delta,t) = \bar{q}(x,\delta,t) = 0$$

$$h_0(x,\bar{w},t) = h_{0_s}(x,t) \qquad p(x,\delta,t) = p_e(x,t) = p_s(x,t)$$

where the subscript "s" indicates conditions at the moving panel surface and the subscript "e" denotes conditions at the unsteady boundary-layer edge. The integration is assumed to take place at a given instant of time as well as at a fixed axial coordinate x so that integrals of the form

$$\int_{\bar{w}(x,t)}^{\delta(x,t)} \frac{\partial Q}{\partial y}\, dy \quad , \text{ where } \quad Q = Q(x,y,t) \quad , \text{ some fluid variable,}$$

can be written immediately as $Q_e(x,t) - Q_s(x,t)$. In order to handle integrals of the form

$$\int_{\bar{w}(x,t)}^{\delta(x,t)} \frac{\partial Q}{\partial x}\, dy \qquad \text{and} \qquad \int_{\bar{w}(x,t)}^{\delta(x,t)} \frac{\partial Q}{\partial t}\, dy$$

we employ an extension of the Leibnitz rule to handle integrals that depend on more than one parameter. The appropriate formula is given by Osgood (Ref. 10) and can be written in the present notation as

$$\frac{\partial}{\partial x}\int_{\bar{w}(x,t)}^{\delta(x,t)} Q(y;x,t)\,dy = \int_{\bar{w}}^{\delta}\frac{\partial Q}{\partial x}\,dy + Q(\delta;x,t)\frac{\partial \delta}{\partial x} - Q(\bar{w};x,t)\frac{\partial \bar{w}}{\partial x} \tag{4.5}$$

$$= \int_{\bar{w}}^{\delta}\frac{\partial Q}{\partial x}\,dy + Q_e\frac{\partial \delta}{\partial x} - Q_s\frac{\partial \bar{w}}{\partial x}$$

$$\frac{\partial}{\partial t}\int_{\bar{w}(x,t)}^{\delta(x,t)} Q(y;x,t)\,dy = \int_{\bar{w}}^{\delta}\frac{\partial Q}{\partial t}\,dy + Q(\delta;x,t)\frac{\partial \delta}{\partial t} - Q(\bar{w};x,t)\frac{\partial \bar{w}}{\partial t} \tag{4.6}$$

$$= \int_{\bar{w}}^{\delta}\frac{\partial Q}{\partial t}\,dy + Q_e\frac{\partial \delta}{\partial t} - Q_s v_s$$

where the limits $\bar{w}$ and δ are considered constants for the integrals on the right-hand sides of the equations. Application of these formulas to the integral form of the boundary-layer equations yields the following result:

$$\frac{\partial}{\partial t}(\rho_e \delta_1) + \frac{\partial}{\partial x}(\rho_e u_e \delta^*) = \Delta\left[\frac{\partial \rho_e}{\partial t} + \frac{\partial}{\partial x}(\rho_e u_e)\right] + \rho_e(v_e - v_s - u_e\frac{\partial \bar{w}}{\partial x}) \tag{4.7}$$

$$\frac{\partial}{\partial t}(\rho_e u_e \delta^*) - u_e\frac{\partial}{\partial t}(\rho_e \delta_1) + \rho_e u_e \delta^*\frac{\partial u_e}{\partial x} + \frac{\partial}{\partial x}(\rho_e u_e^2 \theta) \tag{4.8}$$

$$= \rho_e\,\Delta\left[\frac{\partial u_e}{\partial t} + u_e\frac{\partial u_e}{\partial x} + \frac{1}{\rho_e}\frac{\partial p_e}{\partial x}\right] + \bar{\tau}_s$$

$$\frac{\partial}{\partial t}[\rho_e(h_{0_e}-h_{0_s})\delta_h^*] - (h_{0_e}-h_{0_s})\frac{\partial}{\partial t}(\rho_e\delta_1) + \rho_e\delta_1\frac{\partial h_{0_s}}{\partial t} + \rho_e u_e\delta^*\frac{\partial h_{0_e}}{\partial x} \tag{4.9}$$

$$+ \frac{\partial}{\partial x}[\rho_e u_e(h_{0_e}-h_{0_s})\theta_h] = \rho_e\Delta[\frac{\partial h_{0_e}}{\partial t} + u_e\frac{\partial h_{0_e}}{\partial x} - \frac{1}{\rho_e}\frac{\partial p_e}{\partial t}] - \bar{q}_s$$

The following relations define the displacement thickness δ^*, the momentum thickness θ, the enthalpy thickness θ_h, and two additional thickness variables resulting from the fact that the boundary layer is unsteady:

$$\delta^* = \int_{\bar{w}}^{\delta}(1-\frac{\rho u}{\rho_e u_e})\,dy \tag{4.10}$$

$$\theta = \int_{\bar{w}}^{\delta}\frac{\rho u}{\rho_e u_e}(1-u/u_e)\,dy \tag{4.11}$$

$$\theta_h = \int_{\bar{w}}^{\delta}\frac{\rho u}{\rho_e u_e}(1-\frac{h_0-h_{0_s}}{h_{0_e}-h_{0_s}})\,dy \tag{4.12}$$

$$\delta_1 = \int_{\bar{w}}^{\delta}(1-\frac{\rho}{\rho_e})\,dy \tag{4.13}$$

$$\delta_h^* = \int_{\bar{w}}^{\delta}(1-\frac{\rho(h_0-h_{0_s})}{\rho_e(h_{0_e}-h_{0_s})})dy \tag{4.14}$$

In order to solve for the panel surface pressure distribution the integral boundary-layer equations must be supplemented by additional equations governing the inviscid flow outside the boundary layer as well as relations for $\bar{\tau}_s$ and $\bar{q}_s$ and information for the boundary layer profiles of velocity, density, and total enthalpy. Appropriate boundary conditions must also be specified. A suitable panel displacement amplitude function might be

$$\tilde{w}(x) = \bar{a} \sin kx \ , \quad 0 \leq x \leq a \ ,$$

with additional statements for the remaining variables to be determined.

V. CONCLUDING REMARKS

In connection with hypersonic aerodynamic nonlinearities, the next year's activity will focus on the stability problem. It has already been demonstrated in certain cases that the energy imparted to the panel while fluttering near a linear stability boundary is sufficient to cause an unstable response on the stable side of such a boundary. It would be of interest to fix the initial conditions and see how the linear stability boundary is altered, and then to survey the changes in the altered stability boundary brought about by varying key parameters, such as α' or Mh/a . When this work is completed, the equations will be extended to include rotational edge restraint, up to and including clamped edges.

Work begun on the integral formulation of the unsteady boundary-layer problem for a panel of infinite span will be continued, with the intent of obtaining a mathematically determinate set of equations that can be solved to give the effect of the boundary layer on surface pressure. Some elementary examples will be studied to provide familiarity with the integral approach and to test its generality in predicting viscous effects on surface pressures. A suitable starting point, for example, would be the incompressible flow over a semi-infinite flat plate, or the flow over a small-amplitude rigid wavy wall.

REFERENCES

1. McIntosh, S.C., "Theoretical Considerations of Some Nonlinear Aspects of Hypersonic Panel Flutter," Second Annual Report, NASA Grant NGR 05-020-102, 1 September 1966 to 31 August 1967, Dept. of Aeronautics and Astronautics, Stanford Univ., Stanford, Calif.

2. Dowell, E.H., "Nonlinear Oscillations of a Fluttering Plate," AIAA Journal, Vol. 4, No. 7, July 1966, pp. 1267-1275.

3. Ketter, D.J. and Voss, H.M., "Panel Flutter Analyses and Experiments in the Mach Number Range of 5.0 to 10.0," FDL-TDR-64-6, March 1964, Air Force Flight Dynamics Laboratory, Wright-Patterson AFB, Ohio.

4. Benjamin, T.B., "Shearing Flow Over a Wavy Boundary," Journal of Fluid Mechanics, Vol. 6, Part 2, August 1959, pp. 161-205.

5. Rattaya, J.V. and Volk, E.N., "The Influence of the Boundary Layer on the Perturbed Pressure Over a Flexible or Rigid Wavy Bounding Surface," TM 54/50-72, August 1967, Huntsville Research and Engineering Center, Lockheed Missiles and Space Co., Huntsville, Ala.

6. Zeydel, E.F.E., "Study of the Pressure Distribution on Oscillating Panels in Low Supersonic Flow with Turbulent Boundary Layer," CR-691, February 1967, NASA.

7. McClure, J.D., "On Perturbed Boundary Layer Flows," Rept. 62-2, June 1962, Fluid Dynamics Research Lab., Mass. Inst. of Tech., Cambridge, Mass.

8. Ashley, H. and Landahl, M., "Thickness and Boundary Layer Effects," Manual on Aeroelasticity, AGARD, 1968, Chap. 9.

9. Rasmussen, M.L. and Karamcheti, K., "Viscous Effects Far Downstream in a Slowly Expanding Hypersonic Nozzle," AIAA Journal, Vol. 4, No. 5, May 1966, pp. 807-815.

10. Osgood, W., Advanced Calculus, Macmillan, New York, 1958.

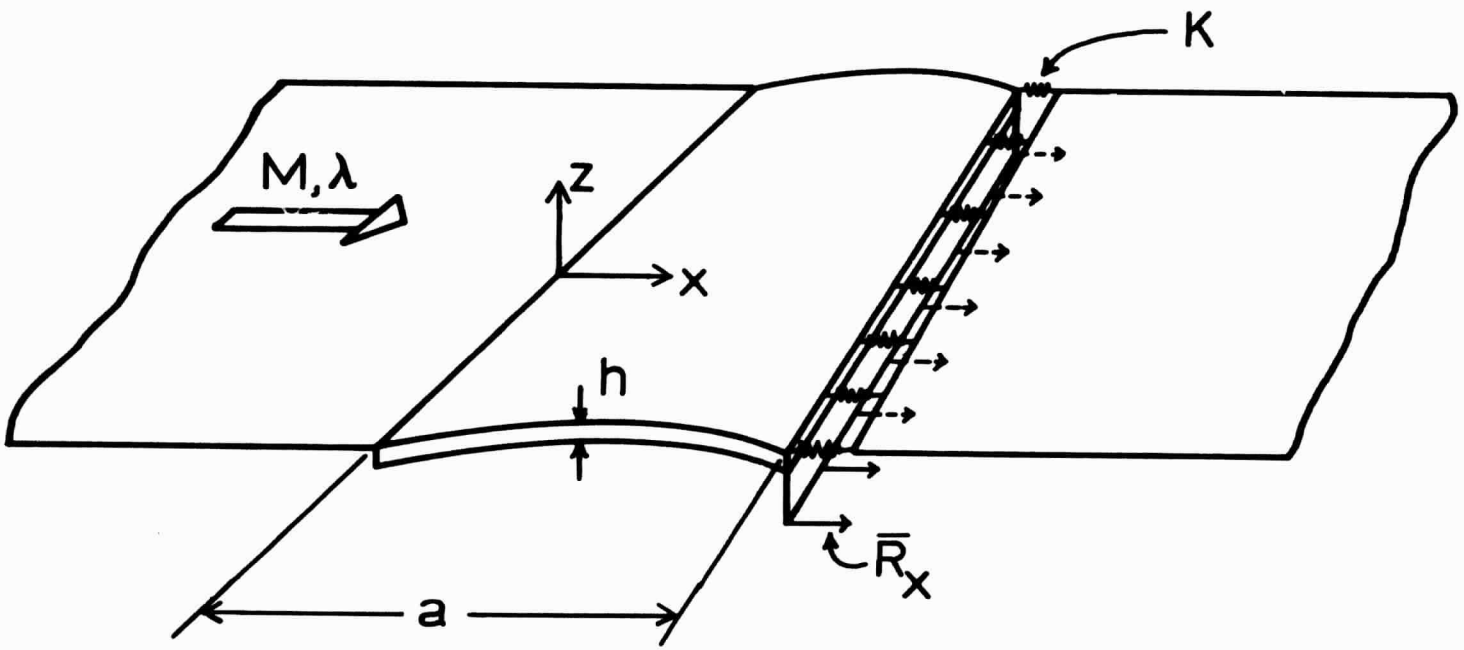

Figure 1. Two-dimensional panel (plate-column) on hinged supports.

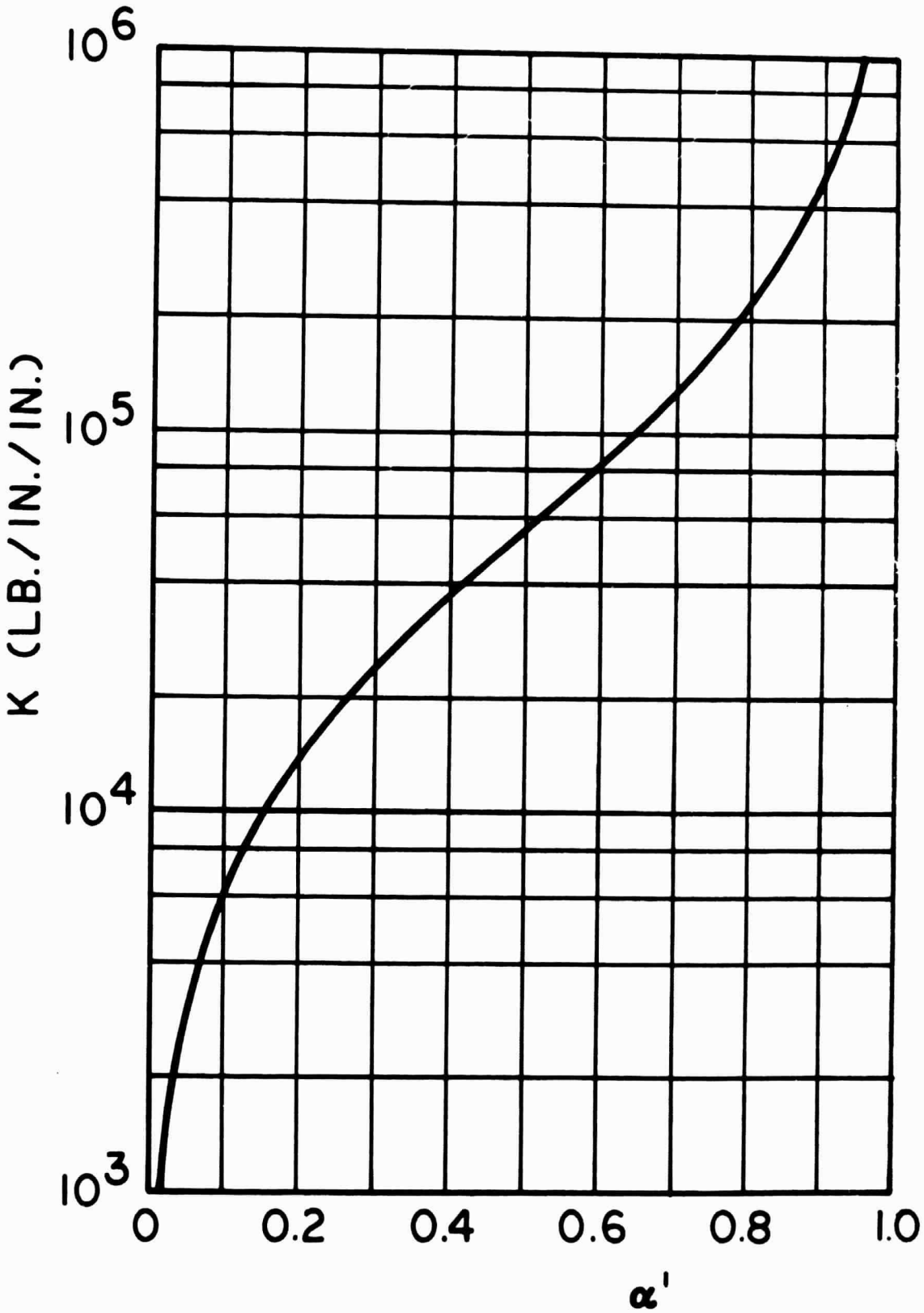

Figure 2. In-plane restraint spring K versus in-plane restraint parameter α' for h/a = 0.005, E = 10^7, ν = 1/3.

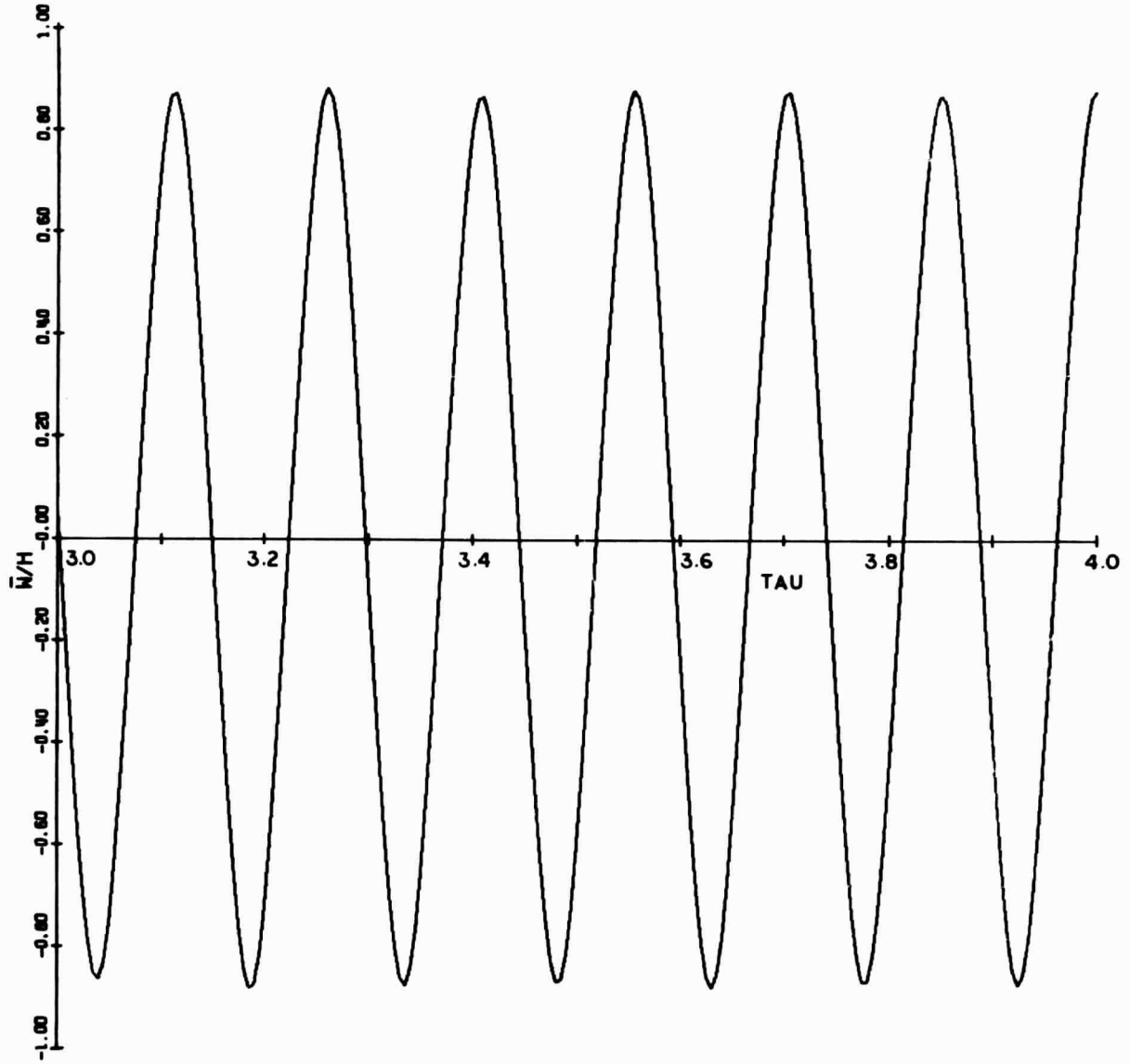

Figure 3. Dimensionless panel displacement w at $x/a = 0.75$ versus dimensionless time τ ; $N = 6$, $\lambda = 550$, $R_x = 0$, $\alpha' = 1$, $\mu/M = 0.01$, $\Delta p = 0$, linear piston-theory aerodynamic loading.

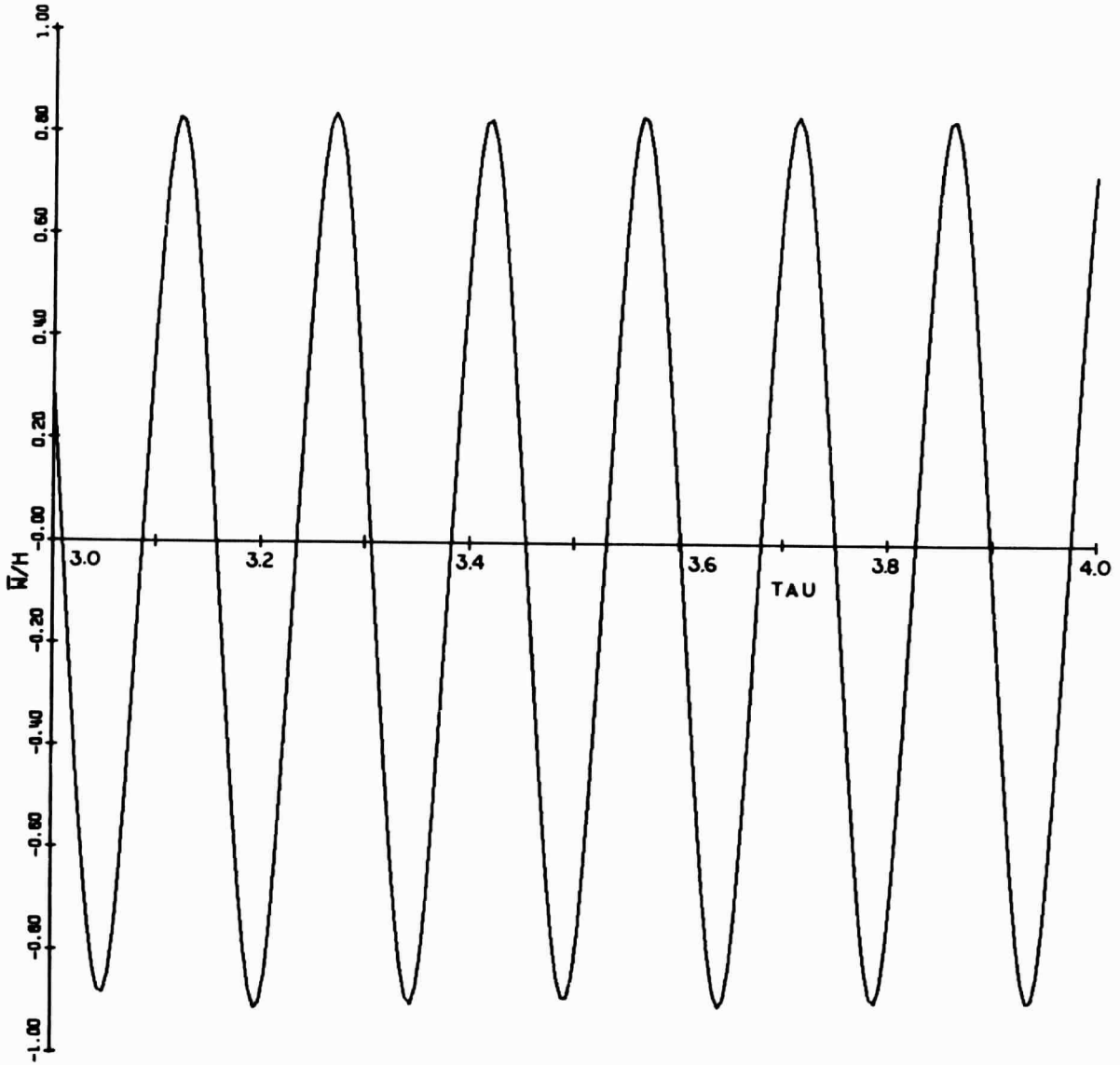

Figure 4. Same plot as in Fig. 3, but with nonlinear piston-theory aerodynamic loading: $Mh/a = 0.05$, terms proportional to $(\partial\overline{w}/\partial x)^2$ and $(\partial\overline{w}/\partial x)(\partial\overline{w}/\partial t)$.

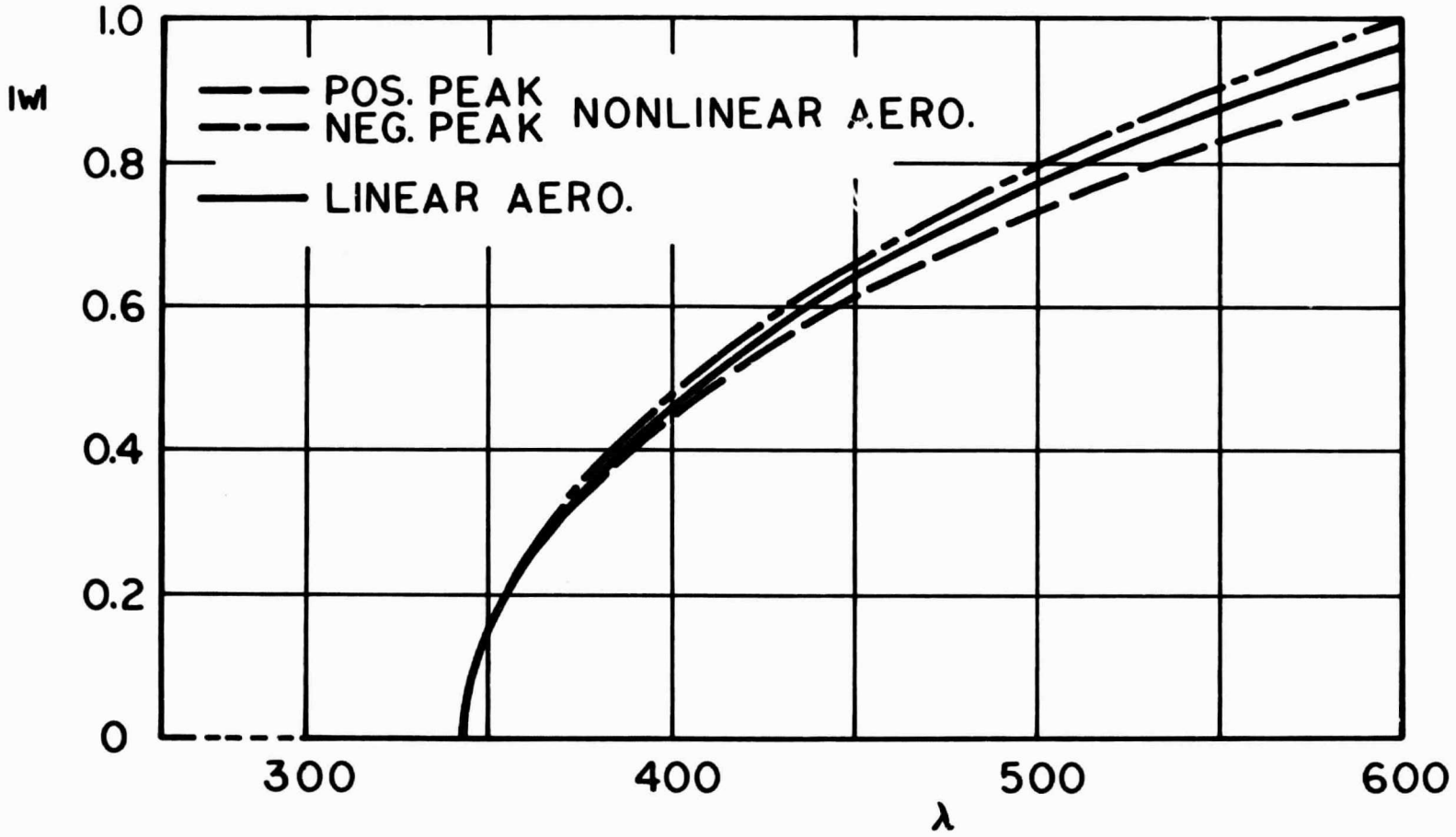

Figure 5. Maximum absolute value of dimensionless panel displacement w at $x/a = 0.75$ versus dimensionless dynamic pressure λ; $N = 6$, $R_x = 0$, $\alpha' = 1$, $\mu/M = 0.01$, $\Delta p = 0$, $Mh/a = 0.05$. Nonlinear aerodynamic loading made up of piston-theory terms proportional to $(\partial\bar{w}/\partial x)^2$ and $(\partial\bar{w}/\partial x)(\partial\bar{w}/\partial t)$.

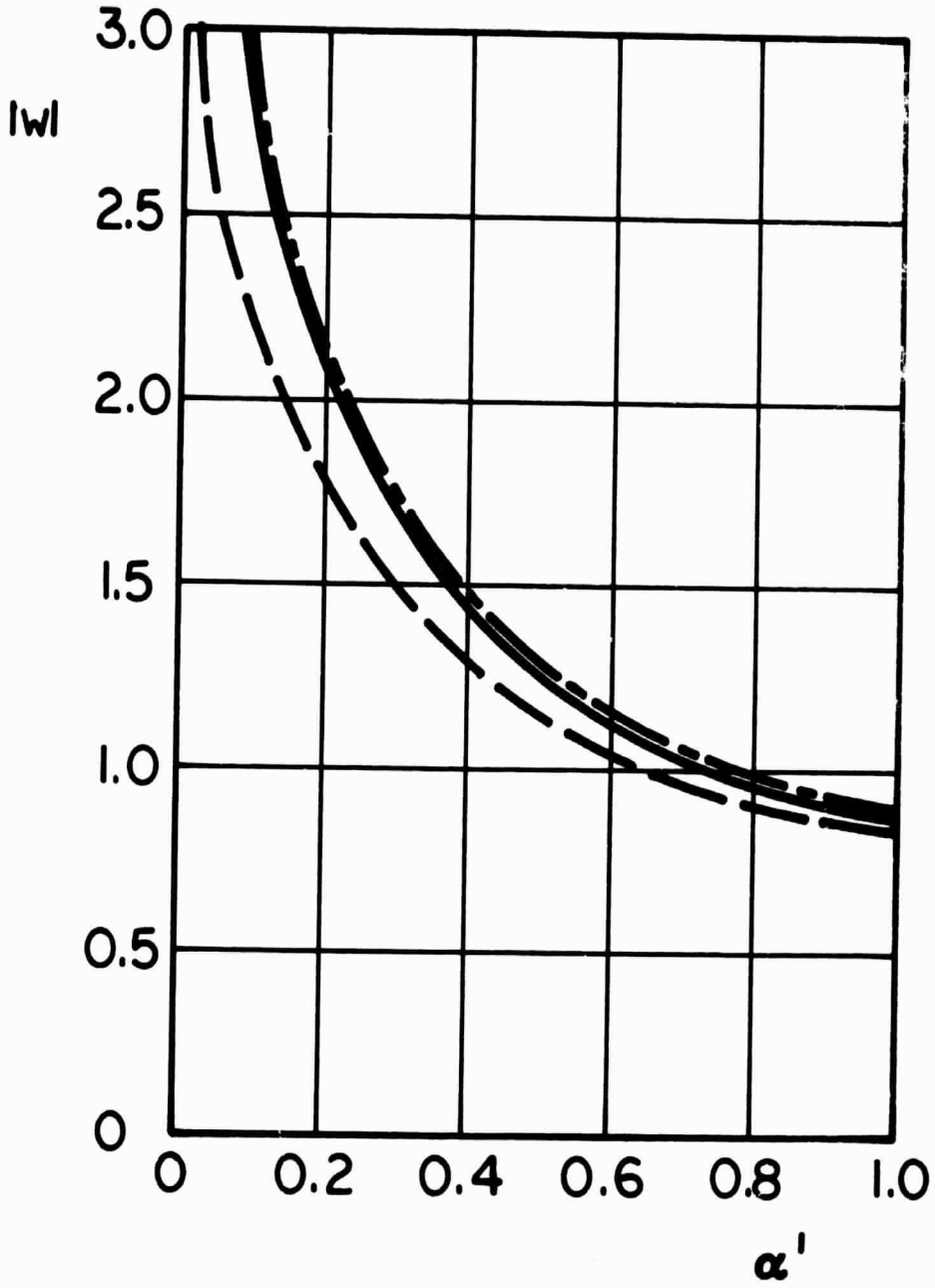

Figure 6. Maximum absolute value of dimensionless panel displacement w at $x/a = 0.75$ versus in-plane restraint parameter α', for $\lambda = 550$. Other parameters and curve legend same as in Fig. 5.

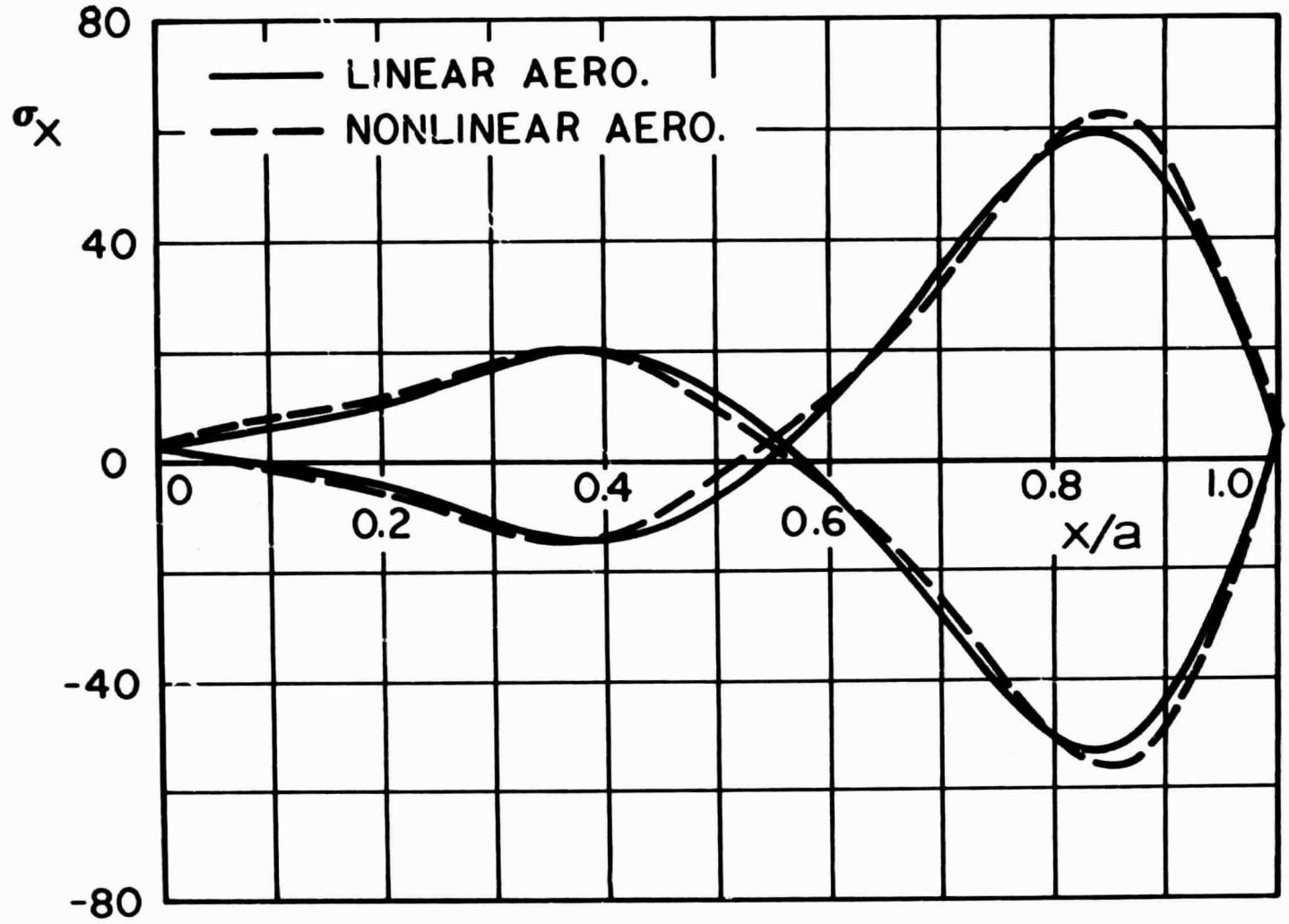

Figure 7. Dimensionless stress σ_x at $z = \pm h/2$ versus chord distance x/a, for $\alpha' = 0.1$, $\lambda = 550$, and other parameters as listed for Fig. 5. Stress distributions correspond to peak displacements plotted in Fig. 6, with that due to nonlinear aerodynamic loading calculated for negative (into-cavity) peak.

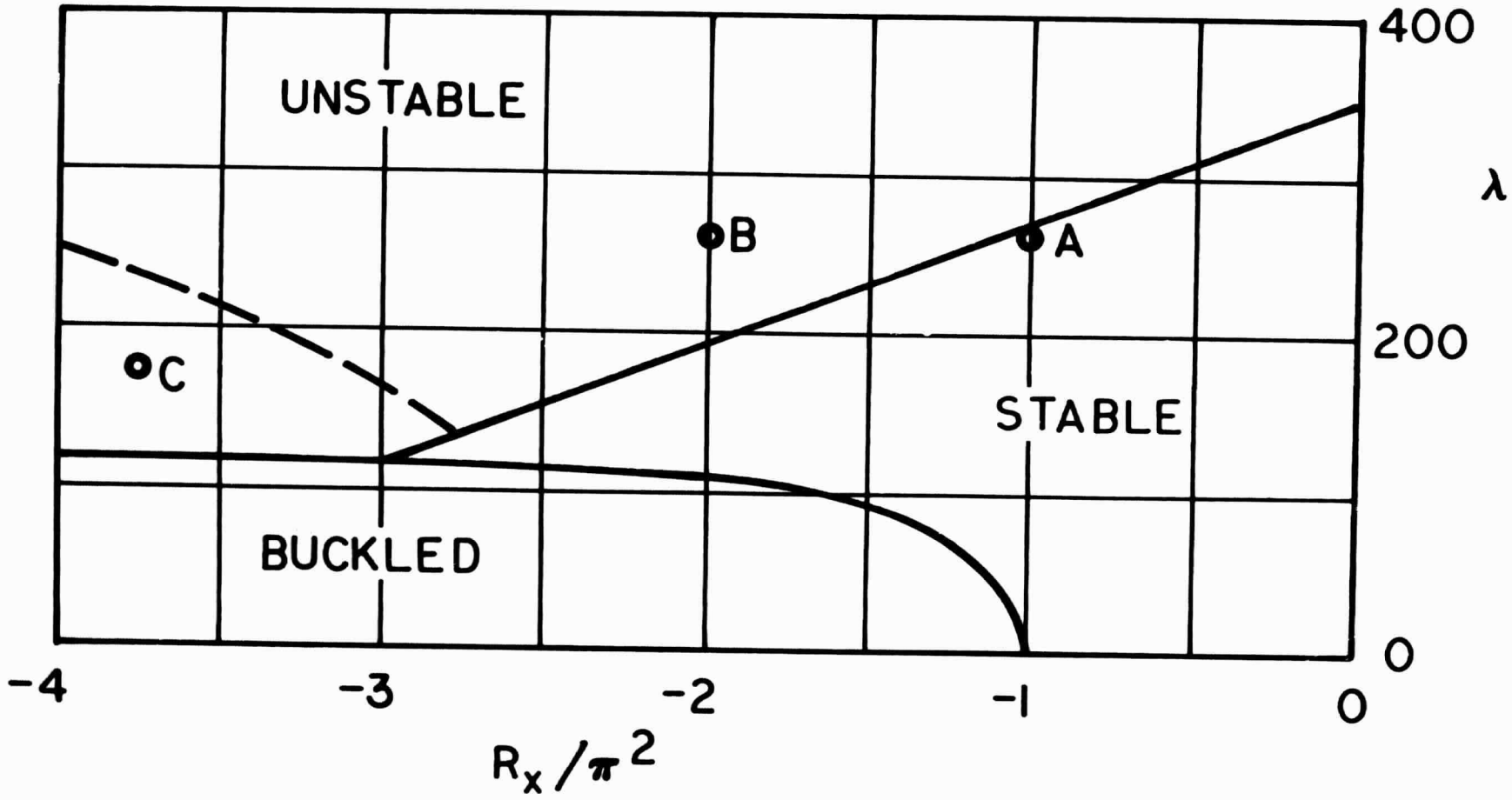

Figure 8. Linear stability boundary for a panel (plate-column) on hinged supports. Ordinate is dimensionless dynamic pressure, abscissa is dimensionless in-plane applied load (negative when panel is in compression). (After Ref. 2.)

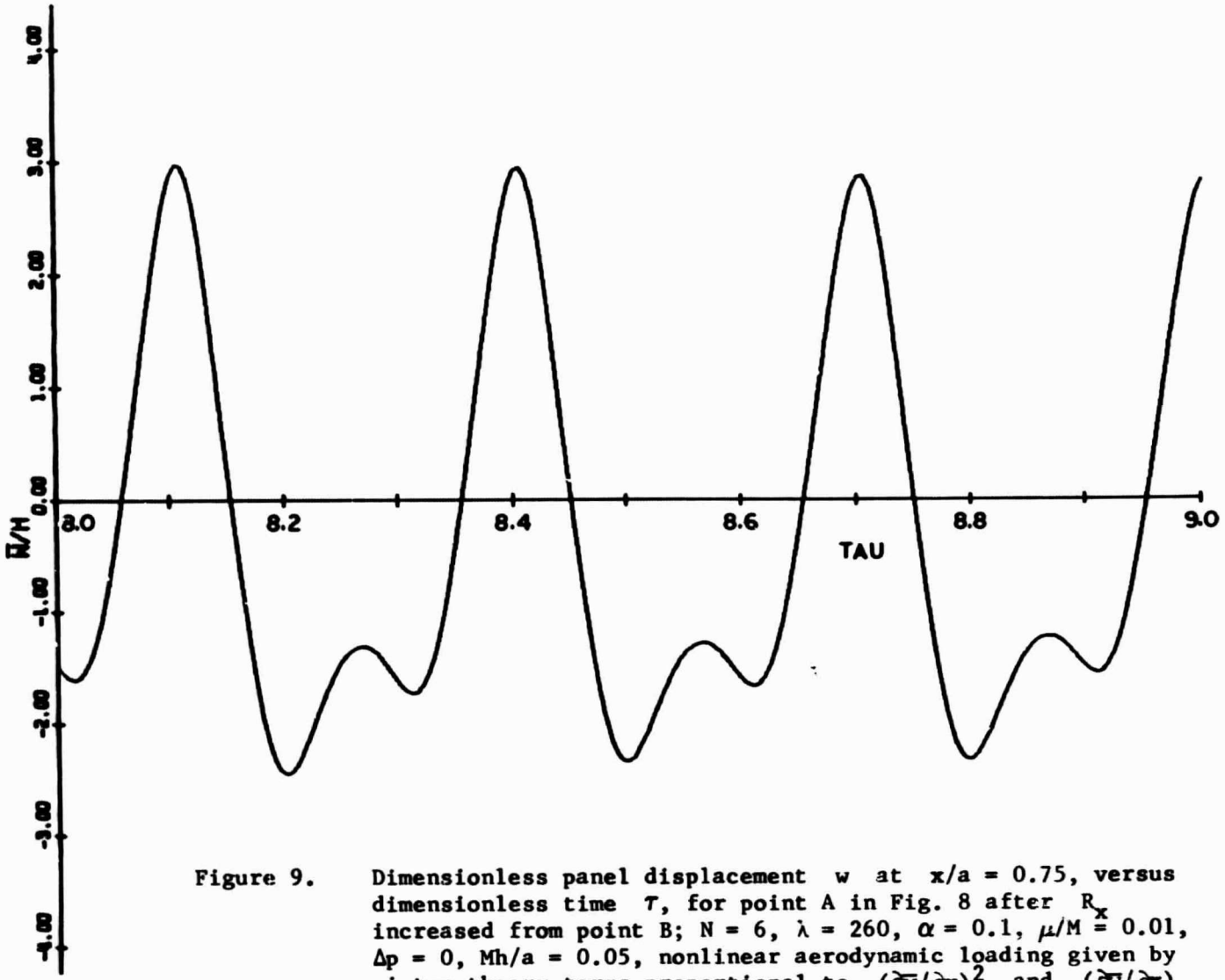

Figure 9. Dimensionless panel displacement w at $x/a = 0.75$, versus dimensionless time τ, for point A in Fig. 8 after R_x increased from point B; $N = 6$, $\lambda = 260$, $\alpha = 0.1$, $\mu/M = 0.01$, $\Delta p = 0$, $Mh/a = 0.05$, nonlinear aerodynamic loading given by piston-theory terms proportional to $(\partial \bar{w}/\partial x)^2$ and $(\partial \bar{w}/\partial x)(\partial \bar{w}/\partial t)$.

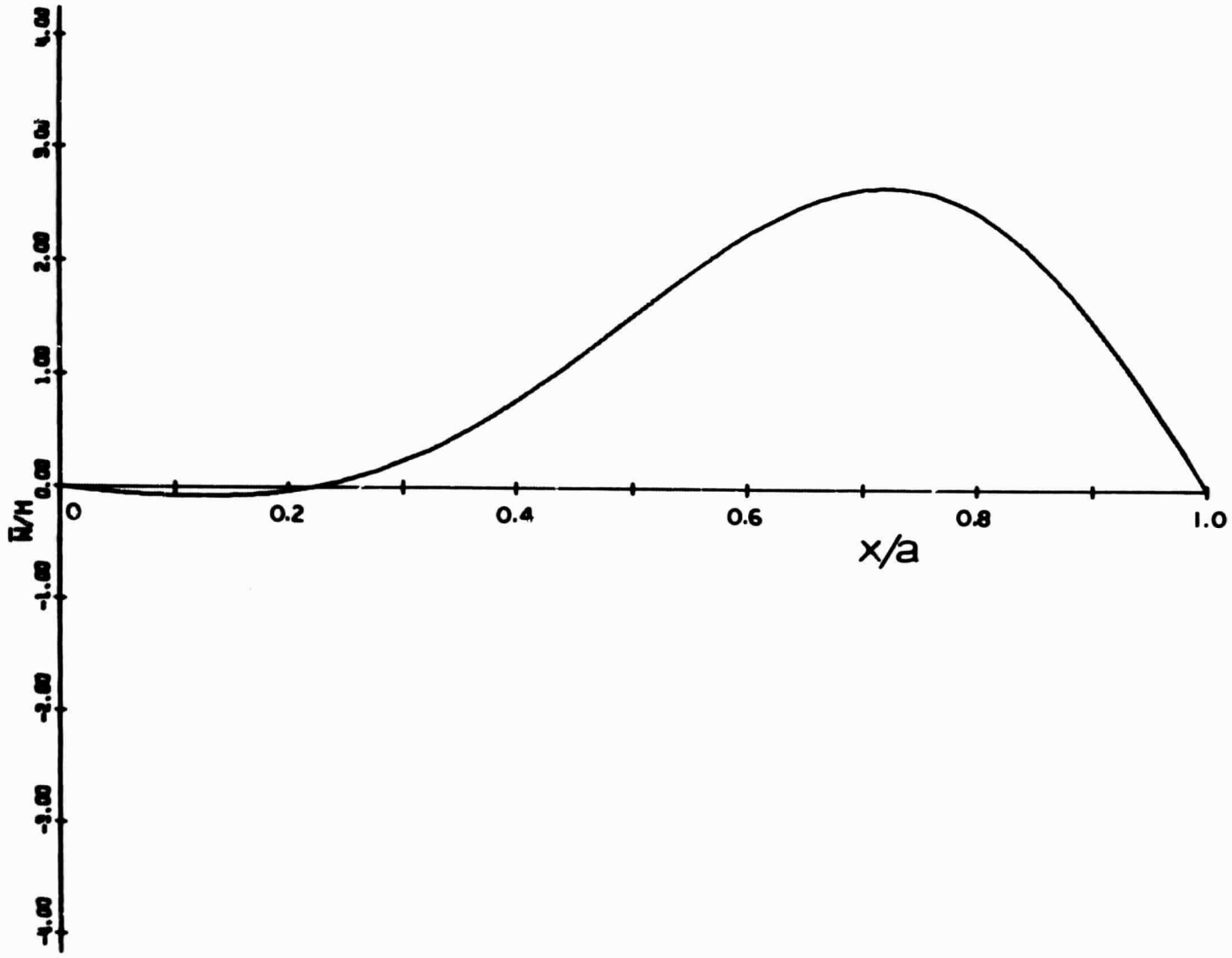

Figure 10. Dimensionless panel displacement w versus chord distance x/a for panel of Fig. 9, $\tau = 8.12$.

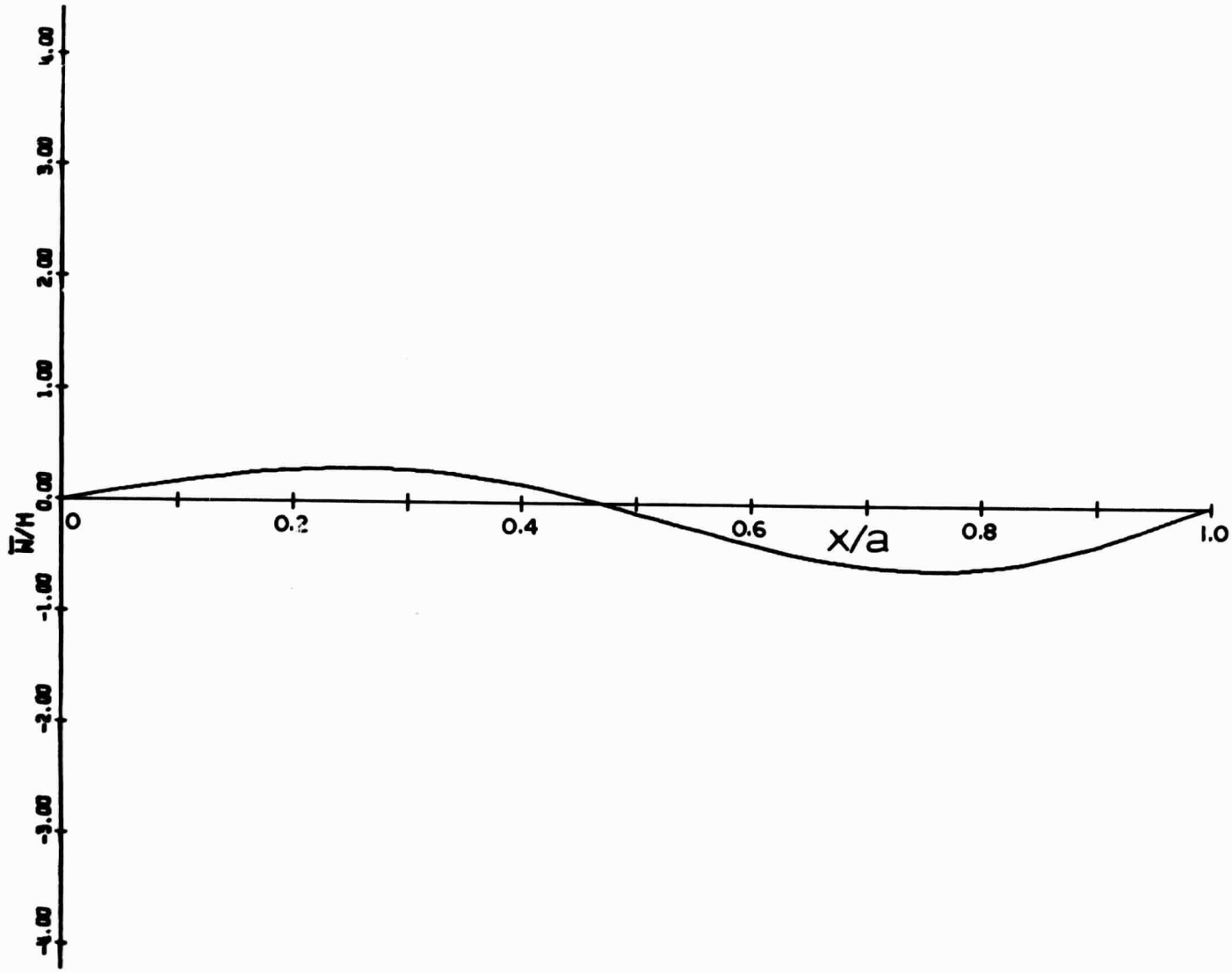

Figure 11. Continuation of Fig. 10, $\tau = 8.16$.

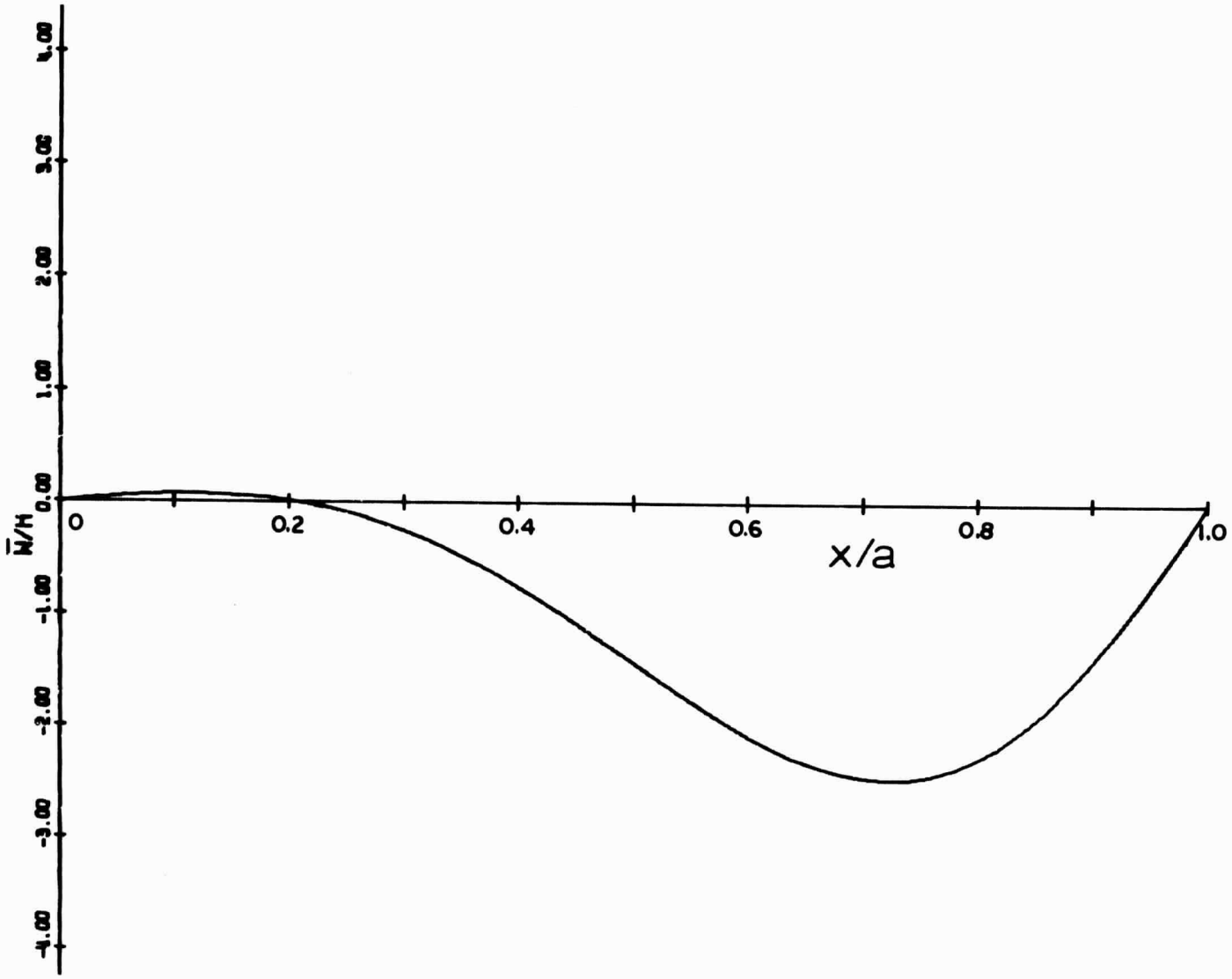

Figure 12. Continuation of Fig. 10, τ = 8.20.

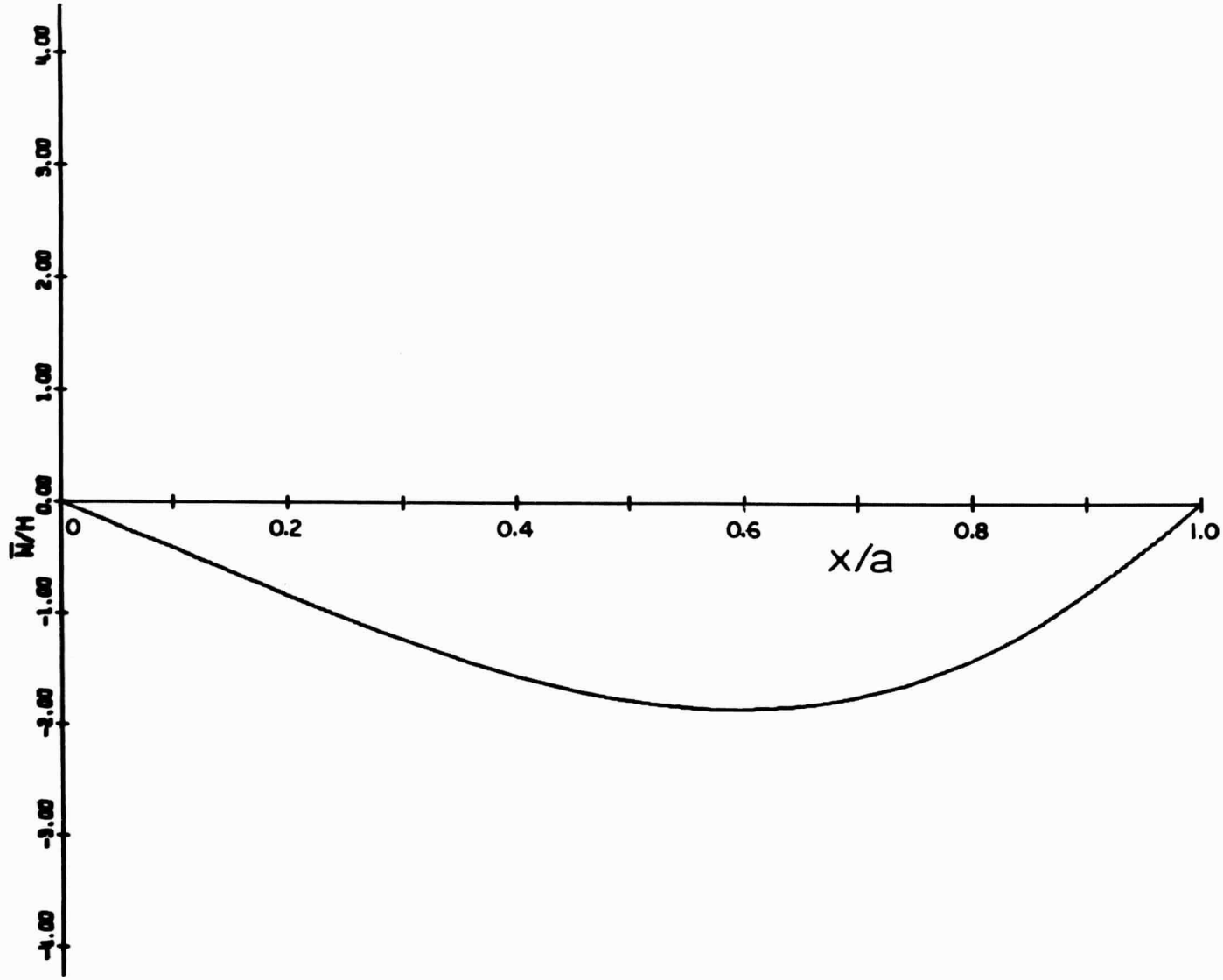

Figure 13. Continuation of Fig. 10, τ = 8.24.

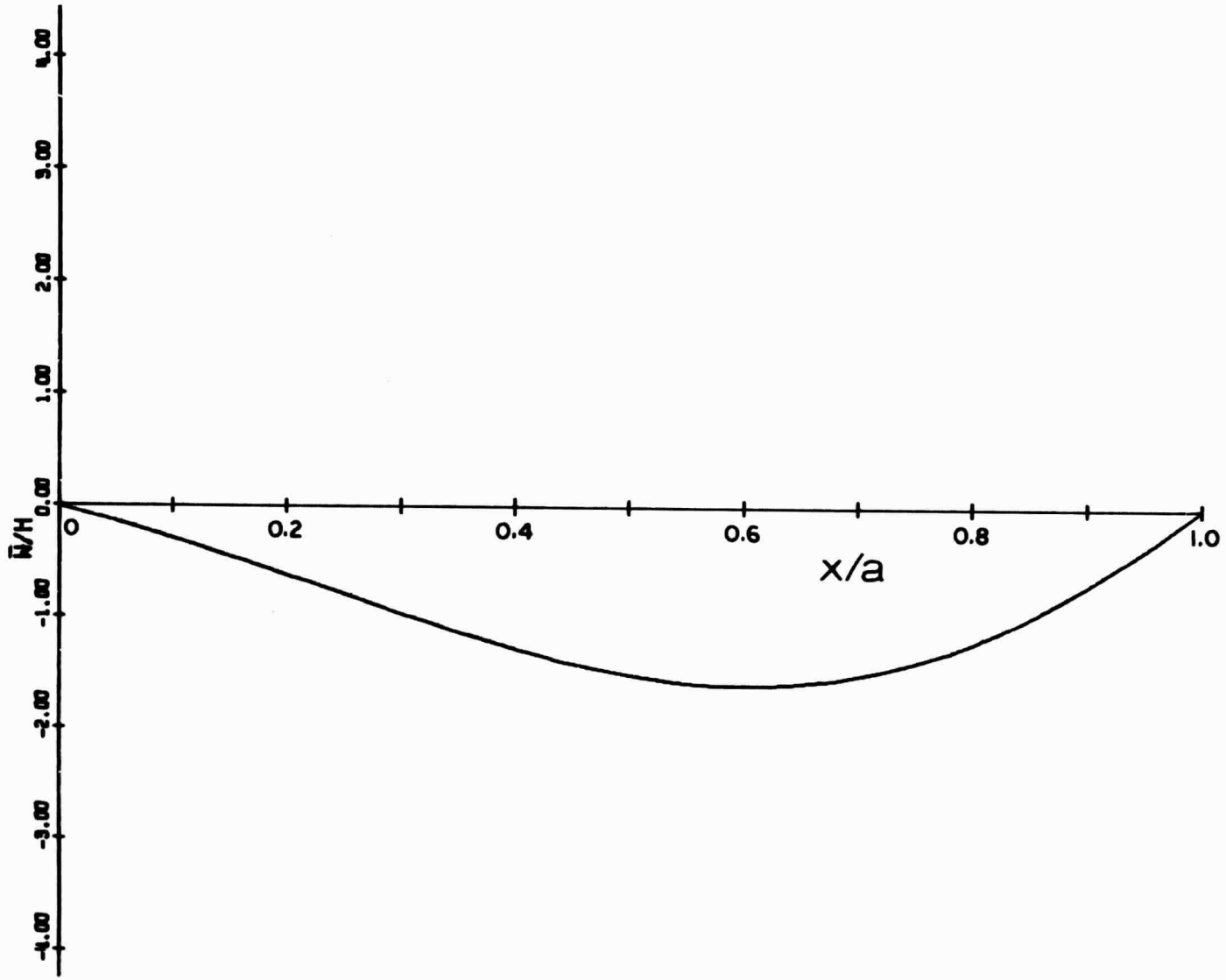

Figure 14. Continuation of Fig. 10, τ = 8.28.

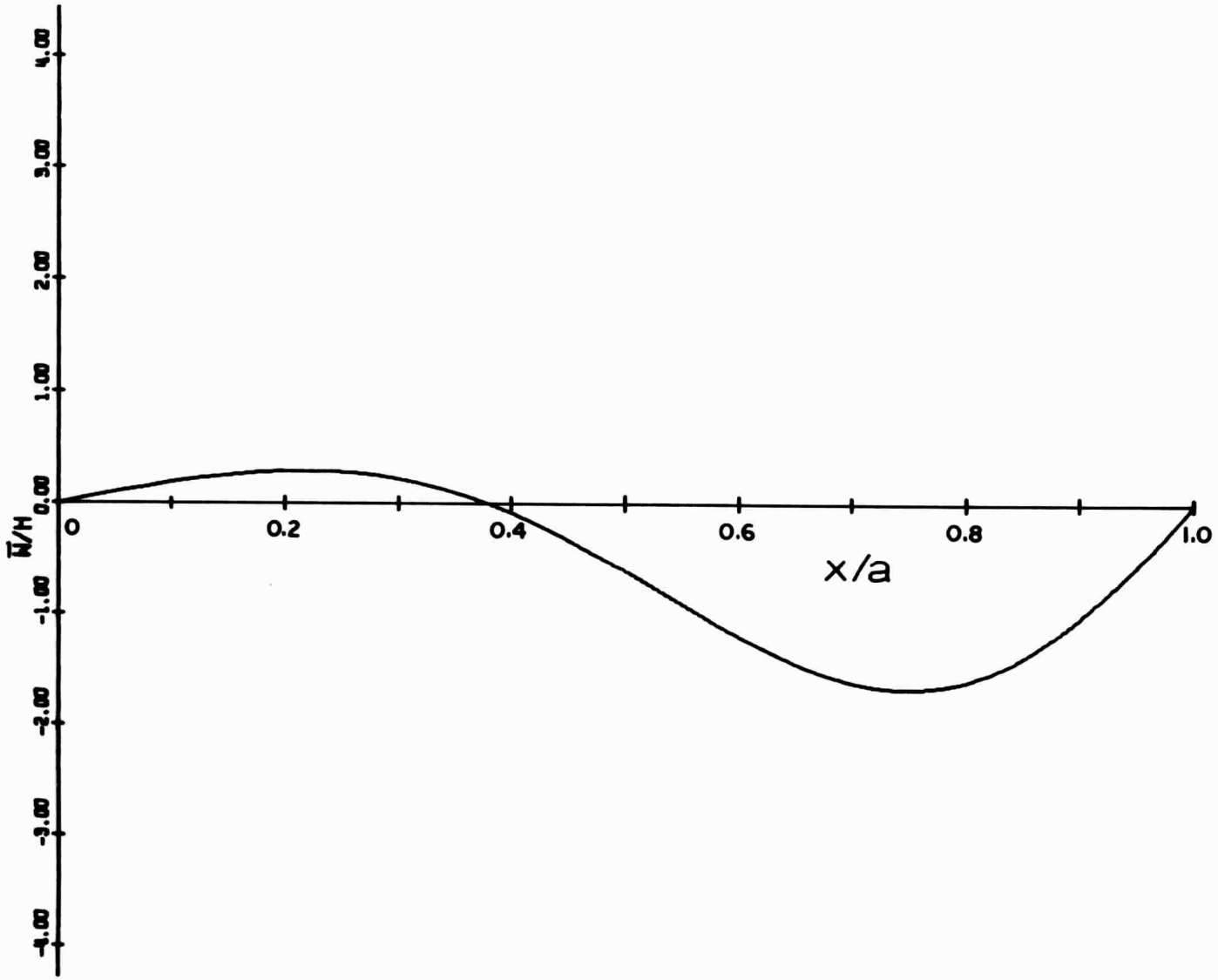

Figure 15. Continuation of Fig. 10, τ = 8.32.

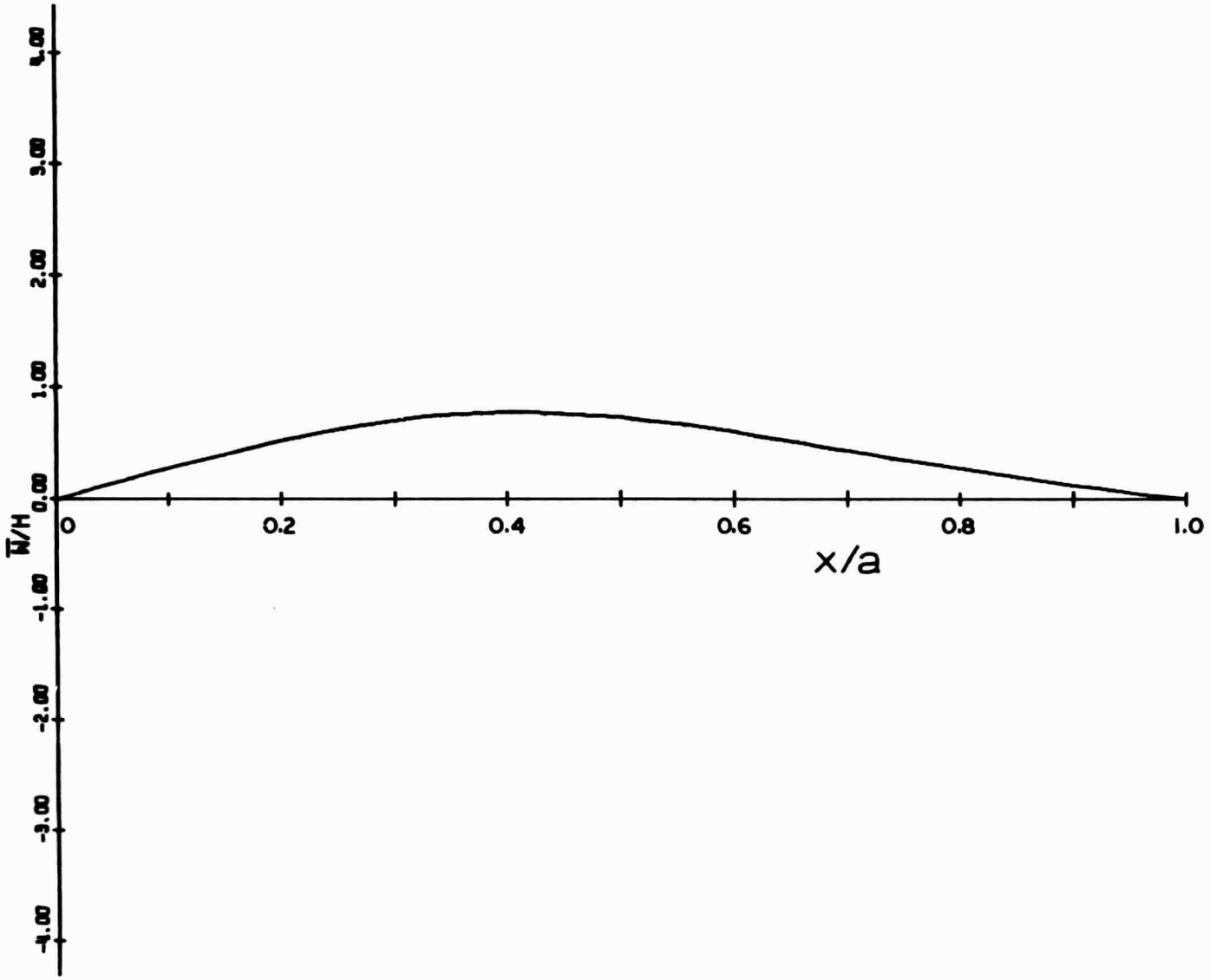

Figure 16. Continuation of Fig. 10, τ = 8.36.

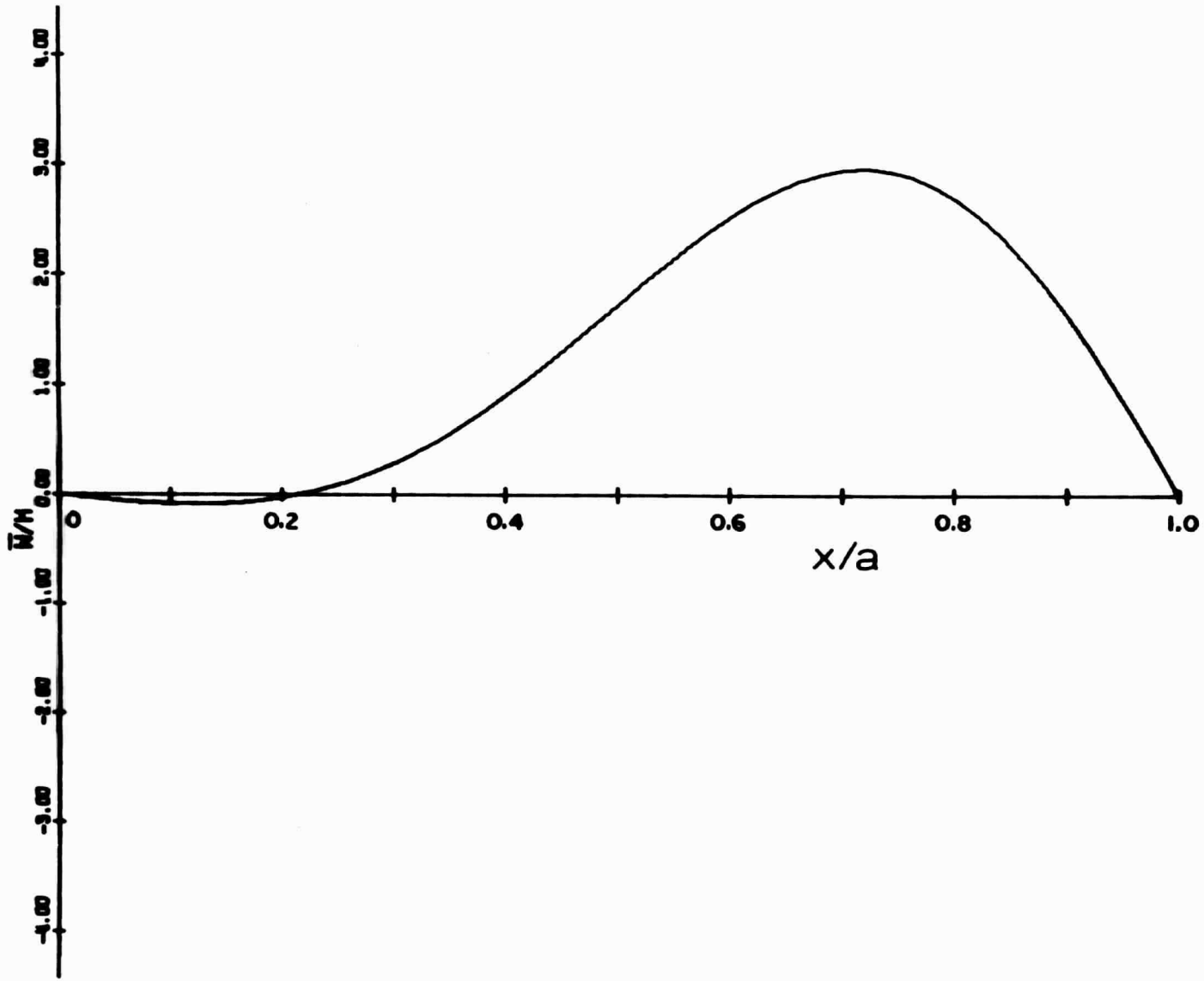

Figure 17. Continuation of Fig. 10, τ = 8.40.

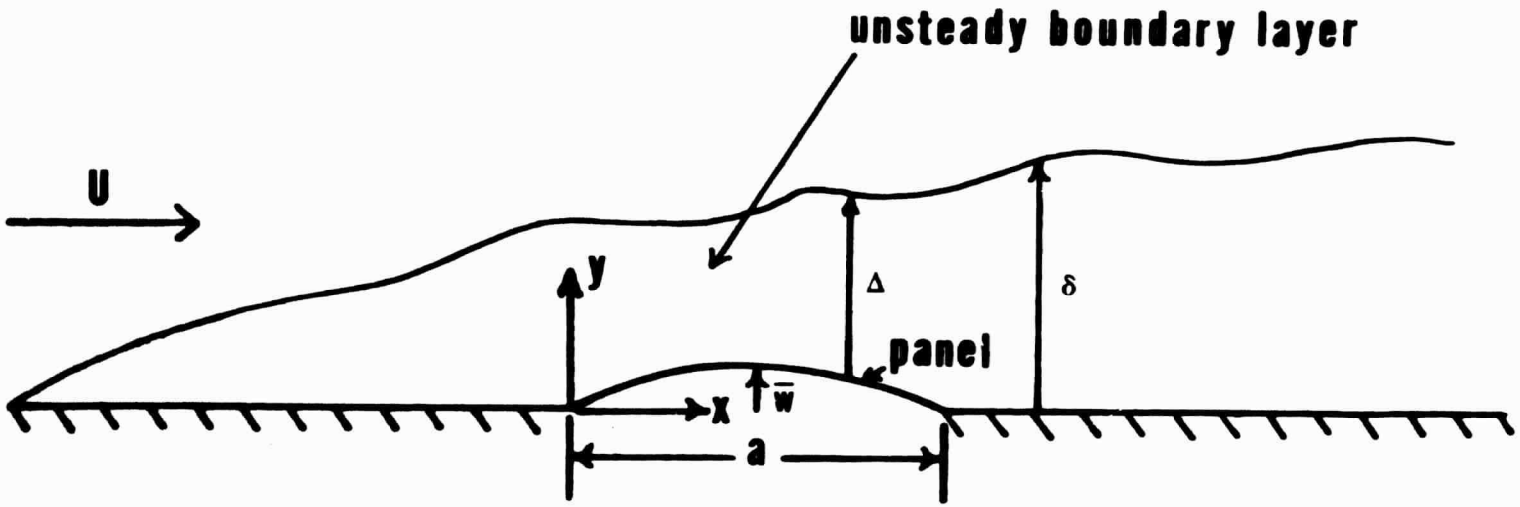

Figure 18. Viscous flow past an oscillating panel (plate-column).